

pubs.acs.org/Macromolecules Article

Li⁺ Conduction in Glass-Forming Single-Ion Conducting Polymer Electrolytes with and without Ion Clusters

Jiacheng Liu and Jennifer L. Schaefer*



Cite This: *Macromolecules* 2023, 56, 2515–2525



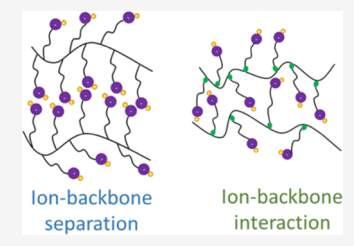
ACCESS

III Metrics & More

Article Recommendations

SI Supporting Information

ABSTRACT: Single-ion conducting polymer electrolytes have been studied for their advantages for rechargeable battery applications. However, amorphous poly(ethylene oxide) (PEO) and related electrolytes are limited by their ion transport rate that is coupled with -EO- segmental motion. Simulations have suggested that fast ion transport may occur within the ion clusters in polymer electrolytes. In this contribution, we report on single-ion conducting polymers with varying polymer backbone types that contain delocalized tethered anions (-sulfonyl-(trifluoromethylsulfonyl)imide (-TFSI $^-$)). The homopolymers were prepared from side-chain monomers capable of free-radical polymerization. The polymer backbone type is found to have strong implications for ion aggregation and nanoscale morphology. A new side-chain ionic polymer



with a nonpolar backbone (polystyrene derivative) is found to self-assemble with lamellar ordering of nanoscale ionic domains. Meanwhile, side-chain ionic polymers with polar backbones (polyacrylate and polymethacrylate derivatives) are found to be less ordered. We show that regardless of the ion aggregation morphology, the bulk ionic conductivity is related to the ionic group relaxation although there are varying degrees of decoupling between thermal glass transition and dielectric relaxation.

INTRODUCTION

High-energy-density secondary batteries are required for many modern applications such as electric vehicles, robotics, internet of things, and personalized electronic devices. Increased safety of the battery while maintaining a fast charging and discharging rate is an important issue to be solved. Solid-state electrolytes, such as polymers and inorganic ceramics and glasses, are expected to decrease flammability and may exhibit mechanical properties to thwart short-circuiting. Inorganic ceramics and glasses can exhibit superionic conductivity but may have drawbacks such as low wettability at electrode interfaces, chemical instability toward moisture and Li metal, and high cost of processing. Polymer electrolytes may be advantageous in these areas. The search for polymer electrolytes with high ionic conductivity and solid-state character is a high priority for future-generation battery development.

A particular class of polymer electrolytes, single-ion conducting polymer electrolytes, is of interest due to their likely high active-ion transference number. The transference number is effectively the fraction of the total ionic conductivity that may be attributed to a particular ion. High transference number electrolytes are sought to mitigate ion concentration gradient formation during battery operation, a phenomenon that can increase interfacial resistance, reduce theoretical limiting currents, and may facilitate lithium dendrite growth with lithium anodes. However, single-ion conducting polymer electrolytes researched thus far suffer from low ionic conductivity.

In the last decade, the ion-hopping transport mode in singleion conducting polymers observed by a series of molecular simulation works has raised interest. ^{9–12} It has been discussed that ionomers with a well-defined chemical architecture can form distinctive ion clusters with various morphologies. ^{13–15} The counterion, usually a monovalent metal ion, can either transfer within ion clusters in a hopping manner or across clusters by ionic group relaxations. ^{9,11} The former mechanism could be a counterpart to ion hopping in ionic glasses, where ion transfer is faster and independent of matrix relaxation. However, the latter mechanism, in general, is dependent on conductivity relaxation like that in glass-forming ionic liquids and polymeric ionic liquids (PILs). ¹⁶

Some recent experimental studies of lithium conducting polyanions with ion clusters have been focused on polymers with a well-defined ionic phase morphology, which are synthesized by step-growth polymerization of prefunctionalized monomers. These polymers are mostly of the main-chain type, on which anions are covalently attached onto or directly pendant to the polymer backbone. Hexagonal, layered, and even gyroid ionic phases have been found in these polymers. More recently, these types of polymers have also demonstrated maintenance of phase separation upon addition of a dimethyl sulfoxide (DMSO) that improves ionic conductivity by up to 10⁴ times. However, due to the limitation of the available polymerization chemistry that is

Received: December 14, 2022 Revised: February 5, 2023 Published: March 16, 2023





compatible with these monomers, investigations of transport in the ionic phase have largely been limited to the sulfonate $(-SO_3^-)$ anion chemistry. Moreover, their ionic conductivity is low in the absence of an organic solvent and the ion transport mechanism remains unclear. Organic solvents may decrease safety or limit use of certain electrodes due to chemical or electrochemical instability; for example, DMSO is reactive with lithium metal anodes.

In our previous works, p-phenylene monomers functionalized by side chains terminated with -sulfonyl-(trifluoromethylsulfonyl)imide (-TFSI⁻) anions were successfully synthesized and polymerized through step-growth. 24,25 These polymers exhibited nanoscale phase segregation, with hexagonal ordering of ionic phases (with side chains of 12 or 15 methylene spacers) or a mixture of hexagonal and lamellar ordering of ionic phases (with side chains of 6 or 10 methylene spacers). The ionic conductivity of all of these side-chain polymers is substantially higher than that of the more common lithiated polyanion (LiPSTFSI), where the tethered anion is immediately pendant to the backbone.²² We showed that the ion transport is coupled with dielectric relaxation, or the ion rearrangement process, although there is some degree of decoupling between the ionic conductivity and calorimetric glass-transition temperature. The decoupling is seemingly from the use of the rigid backbone with flexible side chains, and the more dielectrically susceptible units (the ions) are located at the termini of the side chains. Nonetheless, the achievable polymer architectures are restricted due to the use of this polymer platform.

To further develop the understanding of ion transport within ion clusters in polymers, we expand the strategy to doublebond-type monomers functionalized with anion-terminated side chains that could potentially produce well-defined ionic phases. In this contribution, we report synthesis routes for derivatized styrene, methacrylate, and acrylate monomers that are available for free-radical polymerization, with the potential for living polymerization. The synthesis strategies avoided selfpolymerization of the monomers during intermediate reactions and provided gram-scale final yields. It is found that the polarity of the backbone can impact the morphology, with (meth)acrylate backbones disaggregating ion clusters and exhibiting a broad distribution of correlation lengths in X-ray scattering, while the styrenic backbone supported lamellar ionic clustering. Through the dielectric analysis of the polymers with and without ion clusters, we confirm that the bulk ionic conductivity of both classes of materials is correlated with dielectric (conductivity) relaxation despite presumed differences in the local cation environment.

EXPERIMENTAL METHODS

Materials. 1,10-Dibromodecane (98%), 4-bromophenol (99%), sodium sulfite (≥98%), potassium carbonate (≥99%), potassium iodide (≥99%), oxalyl chloride (≥99%), trimethylamine (>99.5%), 4- (dimethylamino)pyridine (DMAP, ReagentPlus, ≥99%), vinylboronic acid pinacol ester (containing phenothiazine as the stabilizer, 95%), 10-bromo-1-decanol (95%), methacryloyl chloride (≥97.0%), acryloyl chloride (97.0%), palladium(II) acetate (reagent grade, 98%), 2-dicyclohexylphosphino-2′,6′-dimethoxybiphenyl (SPhos, 98%), sodium bicarbonate (NaHCO₃, ACS reagent, ≥99.7%), benzyltriethylammonium bromide (99%), tripotassium phosphate trihydrate (extra pure), acetone (ACS grade), ethanol (ACS grade), 2,2′-azobis(2-methylpropionitrile) (AIBN, 98%), methanol (ACS reagent, ≥99.8%), N,N-dimethylformamide (DMF, anhydrous, 99.8%), tetrahydrofuran (THF, anhydrous, ≥99.9%), dichloromethane

(DCM, anhydrous, $\geq 99.8\%$), hexanes (ACS reagent, $\geq 98.5\%$), Dowex 50WX8 hydrogen form (50–100 mesh), and hydrochloric acid (ACS reagent, 37 wt %) were obtained from Sigma-Aldrich. Trifluoromethanesulfonamide (>98%) was purchased from TCI Chemicals. 1,4-Dioxane (99.8%, extra dry) was purchased from Acros Organics. AIBN was recrystallized from hexanes, and all other materials were used as received. The Spectra/Por 7 dialysis tubing with MWCO 1000 was obtained from Spectrum Laboratories. A Milli-Q system was used to generate deionized (DI) water (18 M Ω).

Synthesis. 1-Bromo-4-((10-bromodecyl)oxy)benzene (1). 4-Bromophenol (13.3 g, 76.8 mmol), 1,10-dibromodecane (23.2 g, 77.1 mmol)), potassium carbonate (9.1 g, 65.8 mmol), potassium iodide (0.5 g, 3.0 mmol), and acetone (320 mL) were loaded in a round-bottom flask equipped with a magnetic stirrer bar. The mixture was refluxed for 12 h with stirring. After the reaction, the reaction mixture was filtered. The acetone was removed under reduced pressure. A white precipitate was collected after adding the resulting oily liquid to hot methanol (150 mL). The product as a white powder was separated by column chromatography (SiO₂, hexanes). Yield: 11.3 g (37%).

¹H NMR (400 MHz, chloroform-*d*) δ 7.35 (d, J = 8.8 Hz, 2H), 6.76 (d, J = 8.8 Hz, 2H), 3.90 (t, J = 6.5 Hz, 2H), 3.40 (t, J = 7.1 Hz, 2H), 1.93–1.68 (m, 4H), 1.51–1.18 (m, 12H).

Sodium 10-(4-Bromophenoxy)decane-1-sulfonate (2). 1 (11.2 g, 28.5 mmol), sodium sulfite (9.1 g, 71.8 mmol), benzyltriethylammonium bromide (0.4 g, 1.5 mmol), ethanol (80 mL), and DI water (80 mL) were charged to a round-bottom flask equipped with a magnetic stir bar. The reaction mixture was refluxed at 95 °C for 48 h. After the reaction, the inorganic precipitate was removed by filtration through analytical filter paper while the mixture was still at the reaction temperature. Then, the collected liquid was allowed to cool down to room temperature overnight to precipitate the product. The precipitate was recrystallized in water and a white powder was obtained. Yield: 9.2 g (77%).

¹H NMR (400 MHz, DMSO- d_6) δ 7.42 (d, J = 9.0 Hz, 2H), 6.90 (d, J = 9.0 Hz, 2H), 3.93 (t, J = 6.5 Hz, 2H), 2.44–2.27 (m, 2H), 1.76–1.61 (m, 2H), 1.62–1.46 (m, 2H), 1.46–1.15 (m, 12H).

Potassium((10-(4-bromophenoxy)decyl)sulfonyl)-((trifluoromethyl)sulfonyl)amide (3). To a dry round-bottom flask equipped with a magnetic stirrer bar, 2 (6.5 g, 15.6 mmol) was suspended in anhydrous THF (40 mL) and cooled in an ice/water bath. Oxalyl chloride (2.38 g, 18.8 mmol), anhydrous DMF (cat.), and anhydrous THF (10 mL) were premixed in a separate container for 30 min and then added to the above suspension under an inert atmosphere. The mixture was stirred for 1 h in the ice/water bath and then at room temperature overnight. Trifluoromethanesulfonamide (2.5 g, 16.7 mmol), triethylamine (4.37 mL, 31.3 mmol), DMAP (0.2 g, 1.6 mmol), and anhydrous THF (30 mL) solution were premixed for 30 min and then added to the above reaction vessel in an ice/ water bath. After addition, the mixture was stirred for 1 h in the ice/ water bath and then at room temperature overnight. After the reaction, the inorganic precipitate was filtered off and the solvent was removed under reduced pressure. The resulting oily liquid was dissolved in DCM (60 mL). The DCM solution was washed with water (3 \times 30 mL), saturated NaHCO₃ (2 \times 40 mL), HCl (1 M, 2 \times 30 mL), and water (3 × 30 mL) and dried over anhydrous MgSO₄ subsequently. After DCM was removed, the resulting viscous liquid was added to the K₂CO₃ (2 equiv) solution to yield the precipitated product. The product was then dried at 60 °C in a vacuum oven for 12 h. Yield: 5.5 g (63%).

¹H NMR (400 MHz, DMSO- d_6) δ 7.42 (d, J = 9.0 Hz, 2H), 6.90 (d, J = 9.0 Hz, 2H), 3.93 (t, J = 6.5 Hz, 2H), 2.97–2.89 (m, 2H), 1.76–1.61 (m, 2H), 1.62–1.46 (m, 2H), 1.46–1.15 (m, 12H).

Potassium((trifluoromethyl)sulfonyl)((10-(4-vinylphenoxy)decyl)sulfonyl)amide (4). 3 (2.6 g, 5.0 mmol), vinylboronic pinacol ester (930.0 mg, 6.0 mmol), palladium acetate (45.4 mg, 0.2 mmol), SPhos (165 mg, 0.4 mmol), tripotassium phosphate trihydrate (4.1 g, 15.3 mmol), and degassed 1,4-dioxane (14 mL) were added to a round-bottom flask under inert argon. Then, the reaction mixture was stirred at 80 °C for 3 h under argon. After the reaction, the mixture was hot-

 Macromolecules
 pubs.acs.org/Macromolecules
 Article

filtered and then allowed to cool down to room temperature. Then, it was diluted with acetone (60 mL). The suspension was filtered, and the liquid phase was collected. The resulting mixture was rotary-evaporated and then purified by column chromatography (SiO_2) acetone/hexanes). The obtained dissolved material in an acetone concentrate was then precipitated twice with hexanes. A yellowish powder was obtained. Yield: 1.4 g (54%).

¹H NMR (400 MHz, DMSO- \bar{d}_6) δ 7.38 (d, J = 8.6 Hz, 2H), 6.89 (d, J = 8.8 Hz, 2H), 6.65 (dd, J = 17.7, 11.0 Hz, 1H), 5.65 (dd, J = 17.7, 1.1 Hz, 1H), 5.09 (dd, J = 10.9, 1.0 Hz, 1H), 3.95 (t, J = 6.6 Hz, 2H), 2.99–2.86 (m, 2H), 1.73–1.60 (m, 4H), 1.47–1.16 (m, 12H). ¹⁹F NMR (376 MHz, DMSO- \bar{d}_6) δ –77.52.

Poly(Lithium((trifluoromethyl)sulfonyl)((10-(4-vinylphenoxy)-decyl)sulfonyl)amide) (LiPSC10TFSI). 4 (0.5 g, 1.0 mmol), AIBN (1 wt %), and DMF (1.2 mL) were charged into a round-bottom flask and degassed by three cycles of freeze-pump—thaw. The reaction mixture was stirred at 68 °C overnight while purging with nitrogen on a Schlenk line. After the reaction, the mixture was diluted in acetone and then dialyzed first in 0.25 M LiCl for three exchanges and then in DI water for three exchanges to remove impurities and exchange to the Li⁺ counterion form. The obtained product was dried in a vacuum oven at 180 °C for 24 h. Yield: 0.23 g (49%).

 1 H NMR (400 MHz, DMSO- d_{6}) δ 7.20–6.20 (m, 4H), 3.98–3.70 (m, 2H), 2.96–2.84 (m, 2H), 2.00–1.00 (m,19H).

Li ICP-OES: 1.44% (found), 1.45% (calc.).

10-Hydroxydecane-1-sulfonate (5). The reaction procedure follows the synthesis of 2, while 10-bromo-1-decanol (15.0 g) was used. The obtained Na^+ product was dissolved in water and passed through a column of Dowex resin (proton form). The product was dried in a vacuum oven at 60 °C to remove water. A waxy solid was obtained. Yield: 13.3 g (62%).

¹H NMR (400 MHz, DMSO- d_6) δ 3.36 (t, J = 6.5 Hz, 2H), 2.50–2.43 (m, 2H), 1.56 (p, J = 7.5 Hz, 2H), 1.43–1.35 (m, 2H), 1.35–1.18 (m, 12H).

Triethylammonium 10-(Methacryloyloxy)decane-1-sulfonate (6). 6 (2.5 g, 11.2 mmol), triethylamine (3.6 mL, 25.7 mmol), and anhydrous DCM (30 mL) were loaded in a dry round-bottom flask under nitrogen protection. The reaction flask was placed in an ice/water bath. Then, the methacryloyl chloride (1.3 g, 12.4 mmol) in anhydrous DCM (15 mL) was added dropwise. The reaction mixture was allowed to stir in the ice/water bath for 2 h and then at room temperature overnight. Then, 10 mL of water was added to the mixture. The oil phase was collected, and the solution was washed with water (15 mL \times 3). A liquid product was obtained after removal of DCM and drying at room temperature over P_2O_5 in a vacuum oven. Yield: 2.1 g (47%).

¹H NMR (400 MHz, DMSO- d_6) δ 9.73–8.39 (s, 1H), δ 6.05–5.97 (m, 1H), 5.71–5.63 (m, 1H), 4.08 (t, J = 6.6 Hz, 2H), 3.09 (q, J = 7.3 Hz, 6H), 2.41–2.32 (m, 2H), 1.63–1.46 (m, 4H), 1.42–1.20 (m, 12H), 1.17 (t, J = 7.3 Hz, 9H).

Potassium((10-(methacryloyloxy)decyl)sulfonyl)-((trifluoromethyl)sulfonyl)amide (7). The reaction procedure follows the synthesis of 3, while 7 (4.0 g) was used. Yield: 1.6 g (34%).

¹H NMR (400 MHz, DMSO- \overline{d}_6) δ 6.05–5.97 (m, 1H), 5.71–5.63 (m, 1H), 4.08 (t, J = 6.9 Hz, 2H), 2.98–2.87 (m, 2H), 1.87 (s, 3H), 1.70–1.54 (m, 4H), 1.42–1.20 (m, 12H).

¹⁹F NMR (376 MHz, DMSO- d_6) δ -77.54.

Poly(lithium((10-(methacryloyloxy)decyl)sulfonyl)-((trifluoromethyl)sulfonyl)amide) (LiPMAC10TFSI). The reaction procedure follows the synthesis of 5, while 8 (1.0 g) was used. Yield: 0.45 g (45%).

 $^{1}\mathrm{H}$ NMR (400 MHz, DMSO- d_{6}) δ 4.09–3.64 (m, 2H), 3.04–2.78 (m, 2H), 1.82–0.58 (m, 21H).

Li ICP-OES: 1.54% (found), 1.56% (calc.).

Triethylammonium 10-(Acryloyloxy)decane-1-sulfonate (8). The reaction procedure follows the synthesis of 7, while acryloyl chloride (2.2 g) was used in lieu of methacyloyl chloride. Yield: 2.3 g (35%).

¹H NMR (400 MHz, DMSO- d_6) δ 9.73–8.39 (s, 1H), δ 6.32 (dd, J = 17.3, 1.6 Hz, 1H), 6.17 (dd, J = 17.3, 10.3 Hz, 1H), 5.93 (dd, J = 10.3, 1.6 Hz, 1H), 4.08 (t, J = 6.6 Hz, 2H), 3.09 (q, J = 7.3 Hz, 6H),

2.41-2.32 (m, 2H), 1.63-1.46 (m, 4H), 1.42-1.20 (m, 12H), 1.17 (t, J = 7.3 Hz, 9H).

Potassium((10-(acryloyloxy)decyl)sulfonyl)((trifluoromethyl)sulfonyl)amide (9). The reaction procedure follows the synthesis of 3, while 9 (1.9 g) was used. Yield: 1.3 g (35%).

¹H NMR (400 MHz, DMSO- d_6) δ 6.32 (dd, J = 17.3, 1.6 Hz, 1H), 6.17 (dd, J = 17.3, 10.3 Hz, 1H), 5.93 (dd, J = 10.3, 1.6 Hz, 1H), 4.08 (t, J = 6.6 Hz, 2H), 2.98–2.86 (m, 2H), 1.74–1.51 (m, 4H), 1.42–1.20 (m, 12H).

¹⁹F NMR (376 MHz, DMSO- d_6) δ -77.53.

Poly(lithium((10-(acryloyloxy)decyl)sulfonyl)((trifluoromethyl)sulfonyl)amide) (LiPAC10TFSI). The reaction procedure follows the synthesis of 5, while 10 (1.2 g) was used. Yield: 0.55 g (46%).

¹H NMR (400 MHz, DMSO- d_6) δ 6.32 (dd, J = 17.3, 1.6 Hz, 1H), 6.17 (dd, J = 17.3, 10.3 Hz, 1H), 5.93 (dd, J = 10.3, 1.6 Hz, 1H), 4.08 (t, J = 6.6 Hz, 2H), 2.98–2.86 (m, 2H), 1.74–1.51 (m, 4H), 1.42–1.20 (m, 12H).

 ^{1}H NMR (400 MHz, DMSO- $d_{6})~\delta$ 4.10–3.68 (m, 2H), 3.07–2.81 (m, 2H), 1.82–0.58 (m, 19H).

Li ICP-OES: 1.60% (found), 1.61% (calc.).

Characterization. ¹H and ¹⁹F NMR spectra were acquired on a Bruker AVANCE III HD 400 Nanobay spectrometer at room temperature with 32 scans. Inductively coupled plasma-optical emission spectroscopy (ICP-OES) was conducted with a Perkin Elmer Optima 8000 system with Prep3 to determine the Li⁺ content. The thermal properties of the side-chain polymers were studied by differential scanning calorimetry. A TA Instrument Q2000 was utilized to monitor the thermal events with a N₂ purge rate at 50 mL/ min. Polymer samples were ramped up to 250 °C and allowed to stand for 5 min to erase thermal history. Then, a cool-and-heat cycle was applied at a ramp rate of 10 °C/min with a lower temperature of -100 °C and without additional isothermal periods. Small- and wideangle X-ray scattering (SAXS/WAXS) tests were conducted at the Advanced Photon Source Synchrotron beamline 12-ID-B run by the Chemical and Materials Science Group at Argonne National Laboratory. Samples were loaded into 1.5 mm (Charles Supper Co.) quartz capillaries in argon atmosphere and sealed with epoxy. The wavelength of the X-ray beam was 0.9322 Å corresponding to 13.3 keV, and the exposure time was 0.1 s. Scattering data was taken upon cooling from 180 °C with 10 min stabilization time at each measurement temperature. Dielectric relaxation spectroscopy was obtained with a Novocontrol broadband dielectric spectrometer coupled with an α -A high-performance frequency analyzer in the range of 1 MHz to 0.1 Hz with an AC amplitude of 0.3 V. The samples were sandwiched between two gold-coated plate electrodes with a diameter of 10 mm, and 50 μ m glass fibers were used as spacers to maintain the sample thickness. Measurements were recorded on cooling, with 10 min stabilization at each temperature. Before testing, samples were conditioned at 180 °C between electrodes to ensure proper contact. Size-exclusion chromatography was recorded with a Waters 1515 Isocratic HPLC, a Waters 2487 Dual λ Absorbance Detector (264 nm), and a Waters 2414 Refractive Index Detector in series with Agilent PolarGel columns (2 × PolarGel-M (mixed pore size; particle size 8 μ m)) and a 1 \times PolarGel-M guard. The samples were eluted using 0.1 M LiCl in dimethylformamide (DMF) at the flow rate of 0.6 mL/minute. Apparent molar masses and molar mass distributions were determined using calibration curves from narrow poly(ethylene glycol) (PEG) calibrants.

■ RESULTS AND DISCUSSION

Chemistry of Side-Chain Single-Ion Conducting Polymer Electrolytes. Synthesis of side-chain single-ion conducting polymer electrolytes with —sulfonyl— (trifluoromethylsulfonyl)imide (—TFSI⁻) anions has rarely been reported because of the harsh condition needed for functionalization. In our previous work, we had synthesized lithiated poly(*para*-phenylene)-based polymers (including LiPPC10TFSI, with 10 methylene spacers on the side chain terminated with —TFSI⁻Li⁺) by Negishi coupling polymer-

Scheme 1. Synthesis Routes for Polymers LiPSC10TFSI, LiPMAC10TFSI, and LiPAC10TFSI

ization.^{24,25} However, the polymer molecular masses are low, which does not favor good mechanical properties, and the ionic mesophase morphology is found to be mostly a hexagonal phase likely due to its linear backbone conformation. Thus, we explore new monomers with double bonds that are available for free-radical polymerization and have potential for living polymerizations. Polystyrene, polymethacrylate, and polyacrylate backbones were chosen for their differences in polarity, homopolymer glass-transition temperatures, and ease of side-chain functionalization.

The synthesis of the polystyrene-derivative (LiPSC10TFSI), polymethacrylate-derivative (LiPMAC10TFSI), and polyacrylate-derivative (LiPAC10TFSI) side-chain polymers with 10 methylene spacers on the side-chain terminated with -TFSI⁻Li⁺ is shown in Scheme 1, and the ¹H NMR spectra for the corresponding monomers are shown in Figure 1. The route for LiPSC10TFSI contains five steps in total, including a sulfonation reaction that requires high temperatures (95 °C) and prolonged time (24 h). This reaction is completed before the formation of the double bond to prevent premature polymerization. A potassium form (rather than Li or Na) of intermediate 3 is preferred because it improves the solubility in 1,4-dioxane and thus increases the reaction yield of the fourth step. In addition, the fourth step using a Suzuki coupling reaction in a relatively mild condition to add the vinyl bond gave satisfactory yield (54%) and avoided premature polymerization. Similarly, the synthesis of LiPMAC10TFSI and LiPAC10TFSI also adapted a sulfonation step before functionalization by the methacrylyl chloride or acryloyl chloride. However, the yield of step 3 is lower, which might be because of the high polarity of the ester group that results in increased loss during the aqueous washing procedure. We did not attempt to optimize the yields.

Size-exclusion chromatography (Figures S1 and S2) shows that LiPSC10TFSI has a weight averaged molecular mass ($M_{\rm w}$) of 62.6 kDa with a dispersity (D) of 3.18, LiPMAC10TFSI has a $M_{\rm w}$ of 125.5 kDa with a D of 4.14, and LiPAC10TFSI has a $M_{\rm w}$ of 24.9 kDa with a D of 2.07. The molecular masses of the newly synthesized polymers are all higher than that of LiPPC10TFSI, with a $M_{\rm w}$ of 18.9 kDa and D of 2.37.

Thermal and Structural Characteristics. The glass-transition temperatures $(T_{\rm g})$ revealed by differential scanning calorimetry (DSC) are presented in Figure 2. The LiPMAC10TFSI displayed a calorimetric $T_{\rm g}$ of 107 °C, which is higher than the $T_{\rm g}$ s of 73 and 62 °C for LiPAC10TFSI and LiPSC10TFSI, respectively. It should be noted that the $T_{\rm g}$ s of poly(methyl methacrylate) and poly(methyl acrylate) are ~105 and ~10 °C, respectively, while the $T_{\rm g}$ of polystyrene is at ~100 °C. As has been discussed in a previous work, the calorimetric $T_{\rm g}$ of LiPPCxTFSI decreases with increasing sidechain length because of enhanced internal plasticizer effect. Similarly, LiPSC10TFSI also presented a lower $T_{\rm g}$ due to the

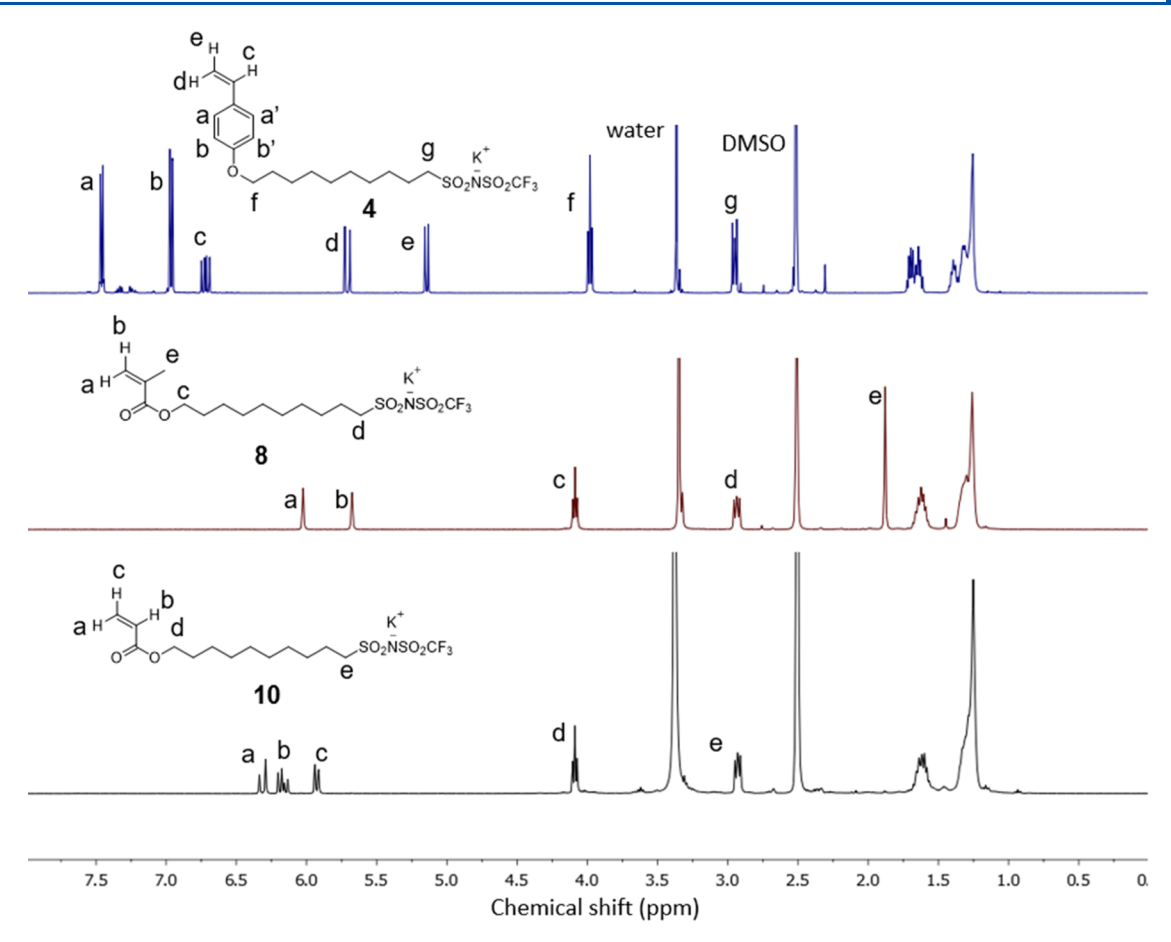


Figure 1. ¹H NMR (in DMSO-d₆) of monomers 4, 8, and 9, and their peak assignments.

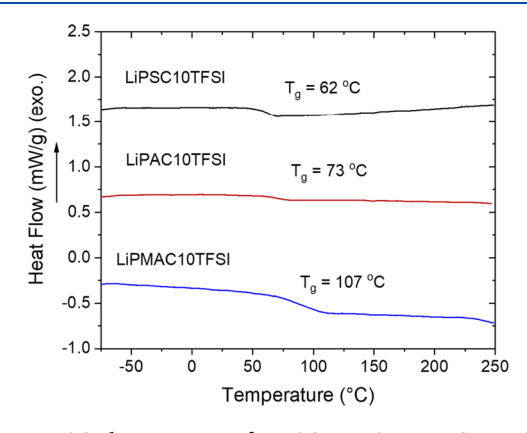


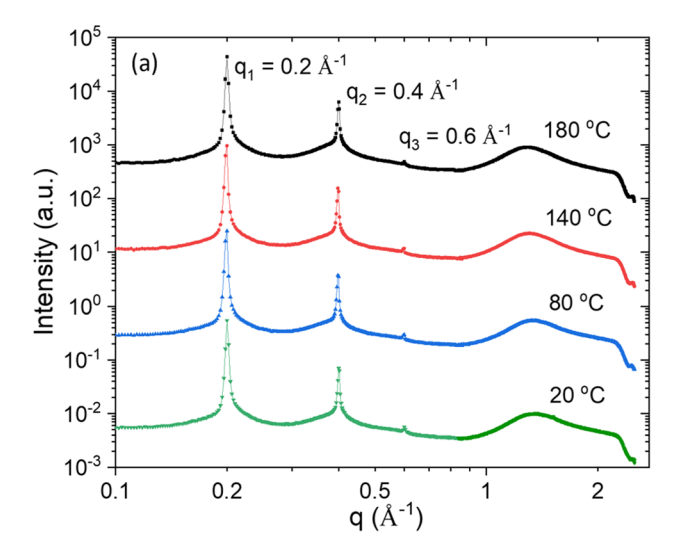
Figure 2. DSC thermograms of LiPSC10TFSI, LiPAC10TFSI, and LiPMAC10TFSI on heating run at the rate of 10 $^{\circ}$ C/min.

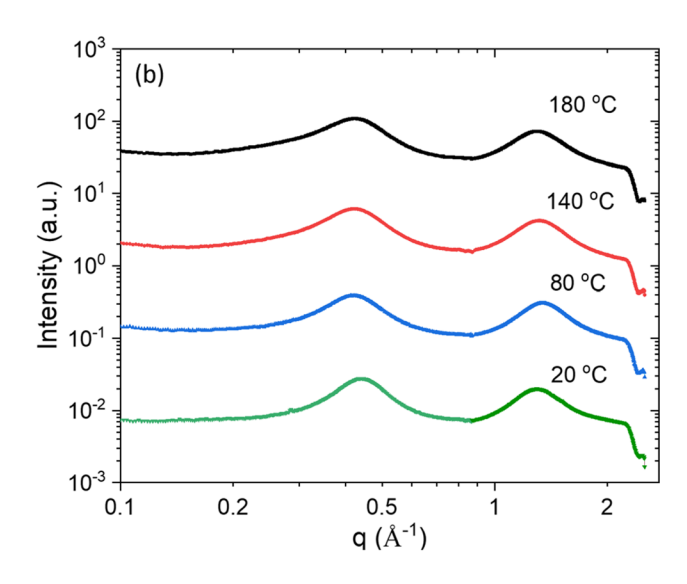
side-chain plasticizer. On the contrary, the $T_{\rm g}$ of LiP-MAC10TFSI did not show such a decline with the same side chain and the $T_{\rm g}$ of LiPAC10TFSI is significantly higher than the underivatized polymer. It has been reported that due to the plasticization effect, the alkyl decyl side chain reduces the $T_{\rm g}$ to -45 °C for poly(decyl methacrylate), 27 and the dynamic shear $T_{\rm g}s$ of poly(decyl acrylate) and poly(decyl methacrylate) are both near -25 °C. 28 Thus, the lack of substantial $T_{\rm g}$ reduction for LiPMAC10TFSI and LiPAC10TF-SI compared with the underivatized polymers can be attributed to the polar–polar interactions added by the ester group on the backbone, which slows down the dynamics and promotes glass-forming in the polymer bulk. 29

The effect of chemical structure on physical properties of LiPSC10TFSI, LiPMAC10TFSI, and LiPAC10TFSI was further elucidated by X-ray scattering. In Figure 3, small-angle X-ray scattering—wide-angle X-ray scattering (SAXS-WAXS) patterns are displayed at various temperatures upon cooling.

LiPSC10TFSI presented distinctive mesophase separation. The polymer exhibits a layered ionic phase morphology represented by peaks at $q = 0.2 \text{ Å}^{-1}$ and so on. The interlayer distance of 3.1 nm suggests that the -TFSI- groups within the layered ionic domains are interdigitated, as this distance is substantially longer than a single monomer unit but shorter than two head-to-head units lacking interdigitation (Figures S15 and S16). It is worth noting that the layered ion clusters are stable even at the highest temperature of 180 °C (453 K), meaning that the interaction between pairs of Li⁺ and -TFSI⁻ is sufficient to preserve the ion clusters from thermal fluctuation. Assuming a spherical assembly of mesophase grains, the Scherrer equation, $d=\frac{2\pi K}{\Delta q}$, where d is the domain size, K = 0.9 is a constant, and Δq is the full width at half height of the primary smectic peak after removal of instrumental broadening, estimates the size of the grain is at the scale of 200 nm.^{30–32} We note that no sharp peak is observed in the high q WAXS region $(q > 1 \text{ Å}^{-1})$, indicating that both the hydrophobic and hydrophilic phases are locally disordered. Therefore, this material may be classified as a thermotropic, polymeric ionic liquid crystal.³³

In contrast, LiPAC10TFSI, which has polar groups on the backbone, displayed a single broad peak in the intermediate *q*-





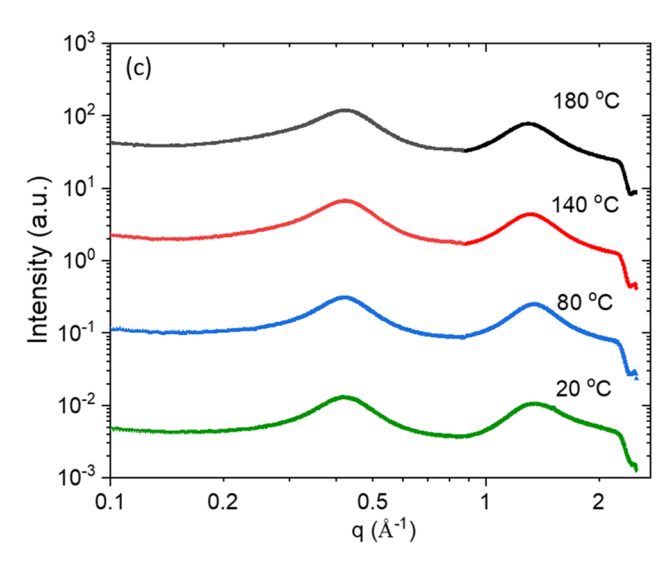


Figure 3. SAXS-WAXS patterns of (a) LiPSC10TFSI, (b) LiPAC10TFSI, and (c) LiPMAC10TFSI recorded on cooling.

region at 0.42 Å⁻¹, indicating an average correlation length of 14.9 Å with a wide distribution. Similarly, LiPMAC10TFSI

showed only a broad peak in the intermediate q-region at 0.44 $Å^{-1}$, indicating an average correlation length of 14.2 Å. This effect has also been discussed by Gin and co-workers that methacrylate monomers prevent ionic molecules from forming an ionic liquid crystalline phase.³⁴ Additionally, MD simulations have indicated that a high dielectric constant results in dissociation of ionic clusters. 11 The phase morphology can also be a function of the hydrophobic content. Previous research has suggested that long paraffin functionality could lead to ion clusters even with more polar ester groups on the polymer backbone. 17 It is reasonable to speculate that methacrylate and acrylate backbone polymers would form ion cluster phases if the methylene spacer content was higher.³⁵ Nanoscale phase segregation is observed for methacrylate and acrylate alkyl side-chain polymers lacking ionic functionalization. ^{28,36} Both LiPAC10TFSI and LiP-MAC10TFSI also exhibit a broad peak in the high q WAXS region, indicating both the hydrophobic and hydrophilic phases are locally disordered in these polymers.

lonic Conductivity. The direct current (dc) ionic conductivity of the polymers was determined by taking the plateau value of the real part of the dielectric conductivity spectrum, and the conductivity values as a function of temperature are shown in Figure 4.³⁷ At 110 °C,

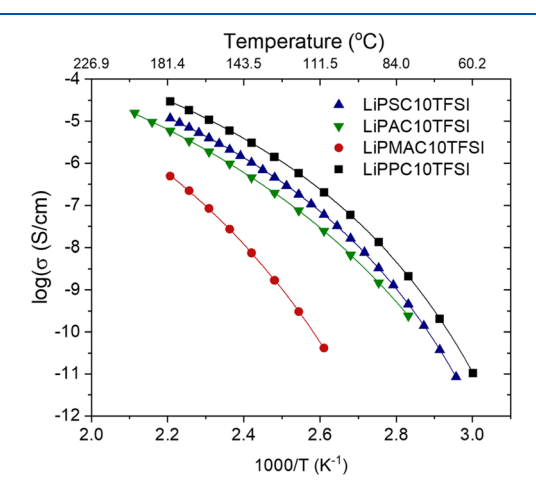


Figure 4. Temperature-dependent ionic conductivities of LiPSC10TFSI, LiPAC10TFSI, LiPMAC10TFSI, and LiPPC10TFSI. Lines represent VFT fits. The data for LiPPC10TFSI was originally published in ref 24.

LiPMAC10TFSI, LiPSC10TFSI, LiPAC10TFSI, and LiPPC10TFSI have conductivities of 4.1 \times 10⁻¹¹, 6.0 \times 10^{-8} , 2.5×10^{-8} , and 2.0×10^{-7} S/cm, respectively. While the conductivities of LiPSC10TFSI, LiPAC10TFSI, and LiPPC10TFSI have similar Vogel-Fulcher-Thammann (VFT) temperature dependencies, LiPMAC10TFSI shows a much lower conductivity and its value decreases faster upon cooling. The reasons for the lower ionic conductivity of LiMAC10TFSI are examined in the following dielectric and ion transport analysis section. The VFT fit parameters are displayed in Table 1 for $\sigma = \sigma_0 \exp(-B/(T - T_0))$, where σ_0 is the pre-exponential factor, B is the pseudoactivation energy, and T_0 is the temperature at which the relaxation time diverges.³⁸ We note that all of the polymers were in their molten state during the experiment because the measurement temperatures are above the DSC $T_{\rm g}$ s. Their ionic conductivities all approached 10^{-12} S/cm at DSC T_{gy} which is higher

Table 1. VFT Fitting Parameters of Conductivity Curves and Glass-Transition Temperatures of LiPSC10TFSI, LiPAC10TFSI, and LiPMA10TFSI

sample	σ_0 (S/cm)	$B (kJ/mol\cdot K)$	T_0 (K)	DRS $T_{\rm g}$ (K)	DSC $T_{\rm g}$ (K)
LiPSC10TFSI	0.065 ± 0.002	6.00 ± 0.04	267	323	335
LiPAC10TFSI	0.204 ± 0.017	8.51 ± 0.13	249	314	346
LiPMAC10TFSI	1.223 ± 0.592	9.55 ± 0.60	274	353	380

than the universal value of 10⁻¹⁵ S/cm for common ionic liquids where the ionic conductivity linearly scales with the structural relaxation rate. Typically, this behavior is attributed to the decoupling effect between structural relaxation and ionic conduction, where the polymeric ionic liquids have high backbone rigidity. 41 The decoupling index has been defined using the formulation $R_0(T_{\sigma}) = 15 +$ $\log \sigma_{\rm dc}(T_{\rm g}).^{42}$ Accordingly, LiPMAC10TFSI, LiPSC10TFSI, LiPAC10TFSI, and LiPPC10TFSI have $R_0(T_\sigma)$ values of 4.6, 3.9, 4.6, and 4.0, respectively. Such a decoupling phenomenon has been observed in several other PIL systems as a result of restricted segmental dynamics. 43

Dielectric and Ion Transport Analyses. Information about dielectric relaxation of LiPMAC10TFSI, LiPSC10TFSI, and LiPAC10TFSI was obtained by fitting the real part of dielectric constant (ε') data to the Havriliak-Negami (H-N)model to elucidate the ion transport mechanism.³⁸ Figure 5

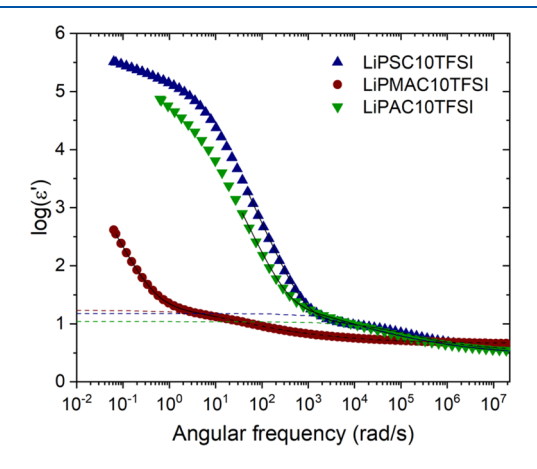


Figure 5. H–N model fitting of the dielectric constant (ε') at 110 °C. Solid lines are fitting of the dielectric relaxation and ion transport. Dashed lines are the contribution of the dielectric relaxation.

presents an example of data processing. The ε' at 110 °C contains three major contributions: electrode polarization at low frequencies, ion transport at intermediate frequencies, and dielectric relaxation at high frequencies. The following equation is used to fit the intermediate to high frequency data.

$$\varepsilon^* = \varepsilon' - i\varepsilon'' = \varepsilon_{\infty} + \frac{\Delta \varepsilon}{\left[1 + (i\tau_{\text{HN}}\omega)^{\alpha}\right]^{\beta}} + \frac{i\sigma}{\varepsilon_0 \omega} + A\omega^{-S}$$
(1)

Here, ε'' is the imaginary dielectric constant, α and β are two shape parameters, $\Delta \varepsilon$ is the dielectric relaxation strength, $\tau_{\rm HN}$ is the H–N relaxation time, ε_0 is the vacuum permittivity, ε_{∞} is the dielectric constant at infinite high frequency, σ is the conductivity, and A and S are two constants. For each sample at each temperature, we found that a single-term H-N fitting can provide satisfactory fitting quality, consistent with our previous examination of the ionic side-chain poly(paraphenylene)s.²⁵ We interpret that the ionic cluster relaxation

of LiPSC10TFSI and local structure rearrangement of LiPMAC10TFSI and LiPAC10TFSI, which are responsible for the observed dc ionic transport, are characterized by very broad time distribution because of the large number of polar groups that are involved in these processes.9 However, the limitation of the frequency range might exclude observation of faster Li⁺ motion such as local hopping or exchange between neighboring positions.

To probe the time constant of the dielectric relaxation behavior, eq 2 is used to calculate the maximum angular frequency (ω_{max}) , or dielectric relaxation rate, by parameters gained from H-N model fitting.

$$\frac{1}{\omega_{\text{max}}} = \tau_{\text{max}} = \tau_{\text{HN}} \left(\sin \frac{\alpha \beta \pi}{2 + 2\beta} \right)^{1/\alpha} \left(\sin \frac{\alpha \pi}{2 + 2\beta} \right)^{-1/\alpha}$$
(2)

As a result, $\omega_{\rm max}$ data are shown in Figure 6. At 110 °C, the $\omega_{\rm max}$ of LiPMAC10TFSI is 30 rad/s, which is $10^{3.3}$ lower than

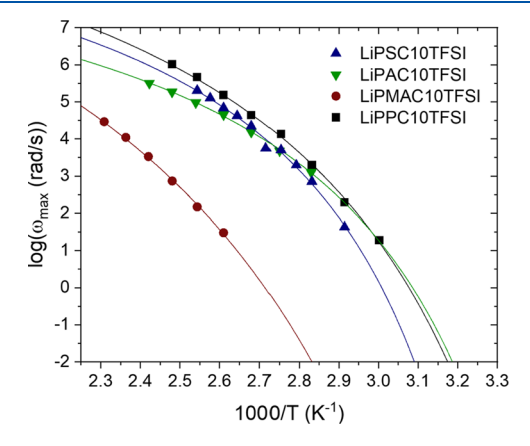


Figure 6. Maximum dielectric relaxation rate (ω_{max}) as a function of inverse temperature. Lines are VFT fits extrapolated to 0.01 rad/s. The data for LiPPC10TFSI was originally published in reference 24.

the 6.9×10^4 rad/s of LiPSC10TFSI. This is similar to the magnitude of difference between their ionic conductivities. It is apparent that LiPMAC10TFSI has a much lower relaxation rate than the other samples, in agreement with the conductivity curves. This result implies that Li+ conductivity in all four of these polymers is governed by the ionic and polar group relaxations. Additionally, the curves in Figure 6 have a similar temperature-dependence as the conductivity. By extrapolating the curves to 0.01 rad/s, we yield the dielectric relaxation glasstransition temperatures (DRS T_g s) for LiPMAC10TSFI as 353 K, LiPSC10TFSI as 323 K, and LiPAC10TFSI as 314 K, a difference with the DSC $T_{\rm g}$ s of 27, 12, and 32 K, respectively. A similar thermal decoupling observation has also been reported in our previous contribution.²⁴ An analogous level of difference between DRS and DSC Tgs has rarely been reported for PIL conductors. While LiPMAC10TFSI and LiPAC10TFSI have a similar chemical structure and morphology, they showed distinctive differences in ionic

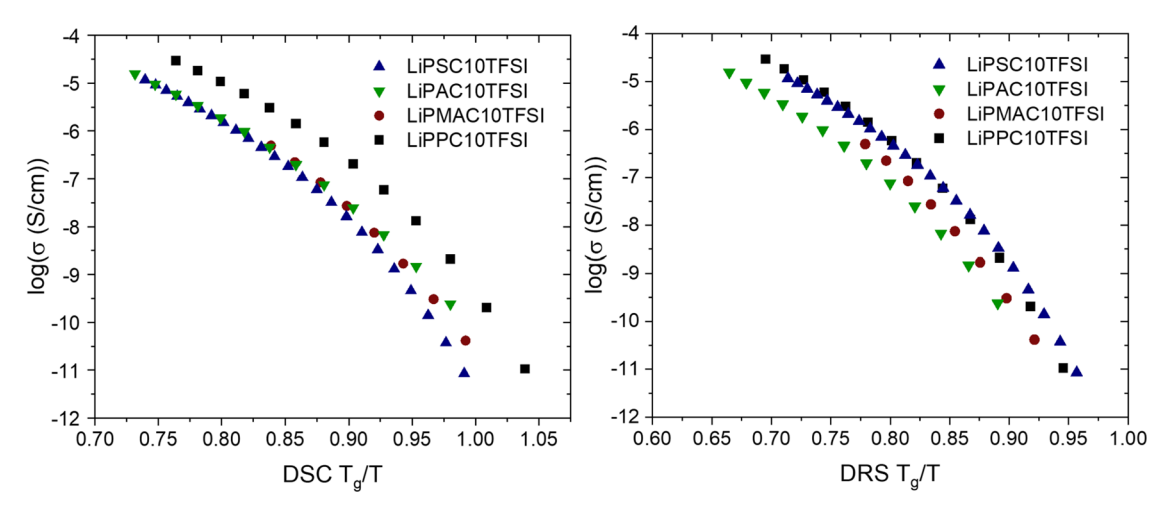


Figure 7. Ionic conductivity plotted against reduced temperatures, (a) reduced by DSC T_g and (b) reduced by DRS T_g . The data for LiPPC10TFSI was originally published in ref 24.

conductivity and relaxation rates as a result of different rigidities provided by the methyl group on the backbone of LiPMAC10TFSI, as shown in both Figures 4 and 6.

DRS $T_{\rm g}$ is more sensitive to ion transport than the overall structural relaxation. ⁴⁴ The difference between DRS and DSC $T_{\rm g}$ s is thus related to the gap between ion transport relaxation and structure relaxation. We hypothesize that the origin of this phenomenon is that the smaller mobile Li⁺ can have more localized jumping, whereas structure relaxation is not required for or the cause of that local ion motion. This situation is in line with the highly fragile PEO-based conductors, where loose packing of rigid polymer chains leads to decoupled Li⁺ motion. ^{45,46} Backbone rigidity has been found to lead to decoupled ion transport in PILs because of frustrated packing and free volume. ⁴¹ In the case of Li⁺, its size is smaller than free ions that have usually been explored in PILs. Thus, it should be easier for Li⁺ to transport in the free volume of the packed ionrich domains here.

To further illustrate the ion transport mechanism in these polymers, the ionic conductivity is presented against normalized temperatures by DSC $T_{\rm g}$ and DRS $T_{\rm g}$, respectively. The level of agreement in the normalized conductivities between samples is an indication of whether the dc conduction mechanism is related to the normalization parameter (here, either DSC $T_{\rm g}$ or DRS $T_{\rm g}$) in the same way between samples.

As shown in Figure 7a, the DSC T_g normalized conductivity of LiPMAC10TFSI is very close to that of LiPSC10TFSI and LiPAC10TFSI. We highlight that a similar conclusion has been made by studying salt-doped PILs with a weakly aggregated morphology in both experiment and simulation, where the DSC T_g normalized conductivity was found to be similar regardless of the extent of ion aggregation.³⁹ The difference in the DSC T_g normalized conductivity for the newly reported polymers compared with LiPPC10TFSI is understood by considering the backbone stiffnesses and interaction of backbones with the conducting species. The backbone of LiPPC10TFSI is highly rigid, yet the structural dynamics are decoupled from the ion dynamics due to the nanoscale phase separation. These combined effects result in the DSC T_{g} normalized conductivity of LiPPC10TFSI being higher than all of the others, regardless of similarity or difference in the ion cluster morphology (and hence the local environment of the cation).

In Figure 7b, where DRS T_g is used for normalization, all four curves are somewhat similar (within an order of magnitude), while data for LiPSC10TFSI and LiPPC10TFSI (both materials with ion clustering) collapse to one common curve. Data in Figure 7b for LiPSC10TFSI and LiPPC10TFSI demonstrate that the ionic group relaxation is responsible for ion transport regardless of the nanoscale ionic phase morphology. VFT-type ionic conductivity has been reported for a wide variety of polymer electrolytes, including mainchain-type ionomers with strong ionic phase separation, where a decent master curve is produced with the glass-transition temperature shifting. 17,19,21,35 More importantly, we report here that polymers with isotropic, layered, and hexagonal ionic phases have nearly common ionic conductivity curves when the temperature is reduced by DRS $T_{\rm g}$. The polymers with more polar backbones and disordered ionic clusters exhibit a lower DRS T_g normalized conductivity, potentially due to the decreased effective number of mobile ions or the contribution of the polar backbone functionalities to the extracted dielectric relaxation.

The static dielectric constant ε_s was obtained by summing $\Delta\varepsilon$ and ε_0 from H–N model fitting and is displayed in Figure 8. The ε_s values for LiPMAC10TFSI and LiPAC10TFSI are similar and higher than those of the other polymers with

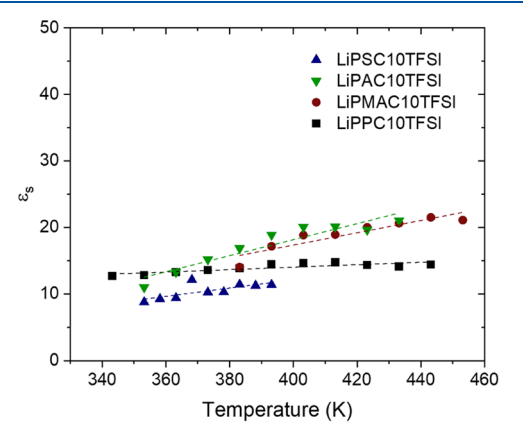


Figure 8. Static dielectric constant (ε_s) of studied polymers at various temperatures. Dotted lines are guides for the eyes. The data for LiPPC10TFSI was originally published in ref 24.

nonpolar backbones. We cannot distinguish if this effect is due to the difference in morphology or the difference in backbone polarity between the polymers. We hypothesize that the strong interaction between Li⁺ and the polar group in these polymers restricts the alignment or reorientation of dipole moments, thus leading to lower ε_s than is commonly observed for PILs. It is observed that ε_s shows an increasing trend as the temperature increases, unlike Onsager predictions where ε_s decreases as the temperature increases. 47,48 The increase of $\Delta \varepsilon$ with temperature in PILs has been attributed to ion-ion correlations and also linked to conductivity relaxation, where the observed dielectric relaxation is dominated by the ion rearrangement process. 49 A similar increase of ε_s with temperature has also been observed in PEO-based ionomers at lower temperatures or a higher ion content, where dipole motion is restricted. 50-52

It is noted that the increased ε_s for the polar polymers does not result in enhanced conductivity. The ester group dissociated ionic aggregates as seen via SAXS, resulting in an isotropic phase and more interactions between the polar backbone and ionic groups. This interaction restricted the ion conductivity because it slows down the relaxation dynamics, which has been studied in amorphous PEO conductors. ⁵³

Barton, Nakajima, and Namikawa (BNN) have proposed a linear scaling theory between ionic conductivity and the dielectric relaxation rate. The BNN relation is empirically described by $\sigma = \varepsilon_0 \omega_{\rm max} \varepsilon_{\rm s}$. Figure 9 displays the resulting scaled

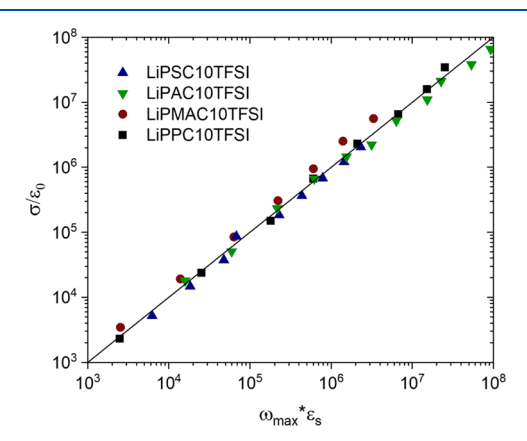


Figure 9. BNN scaling of the studied polymers where the line represents the scaling factor B = 1. The data for LiPPC10TFSI was originally published in ref 24.

plot where all four polymers fit the universal scaling factor B = 1. This result indicates that the ion rearrangement process totally governs the Li⁺ transport in all cases.

■ CONCLUSIONS AND OUTLOOK

In this contribution, we present synthesis methods to achieve single-ion conducting polymer electrolytes with full —TFSILi ion-pair and side-chain spacer functionality. These methods open up the synthesis routes for single-ion, cation-conducting polymer electrolytes with a well-defined ionic phase morphology. The reaction conditions are mild and have the potential to be scaled up. Three kinds of polymerizable functional monomers are reported: styrene, acrylate, and methacrylate types, with different polarities and rigidities of the backbone. In addition to free-radical polymerization used in this study, living polymerization with the reported monomers is expected to

produce narrower dispersity products. The polystyrene-back-bone side-chain ionic polymer is an ionic liquid crystalline polymer that forms stable layered ionic phases over a wide range of temperatures even with a high charge-delocalizing anion (—TFSI⁻). In contrast, the polyacrylate- and polymethacrylate-backbone side-chain ionic polymers have disordered ionic aggregates. This synthesis platform has potential for adoption with various anion chemistries and side-chain architectures, which might affect the phase morphology and counterion transport rate.

The Li⁺ transport mechanism in these side-chain polymers has been correlated with dielectric relaxation, regardless of the degree of ionic aggregation. This mechanism is confirmed by comparing the DRS T_g normalized Li⁺ conductivity among amorphous, smectic, and hexagonal phase polymers with identical side chains. Polymers with ordered ionic phases segregated from the backbones exhibited nearly identical DRS T_{σ} normalized conductivities. Despite the disordered morphology of the polyacrylate- and polymethacrylate- side-chain ionic polymers, where it is expected that there is an interaction between the backbone ester-group and Li+, these polymers exhibit fairly similar real and glass-transition temperature normalized temperature-dependent conductivity profiles to the polymers with segregated ionic clusters. The lowest real ionic conductivity is observed for the polymethacrylate-backbone side-chain polymer and is attributed to the backbone-cation interaction along with slow structural relaxation.

The fast ionic conductivity that is characterized by ion hopping has not been observed in our studies so far. However, these findings do not mean that ion hopping does not exist in single-ion polymers with or without ionic phase separation. Grain boundaries and lack of percolation of ion clusters can hinder the ion hopping, preventing it from contributing to dc conductivity. Ionic phases that persist for a longer length scale with alignment in the direction of the electric field may aid in the investigation of the in-cluster ion-hopping mechanism.

ASSOCIATED CONTENT

Supporting Information

The Supporting Information is available free of charge at https://pubs.acs.org/doi/10.1021/acs.macromol.2c02516.

NMR spectra, size-exclusion chromatography traces for polymers and calibrants, calibration curve, Chem3D predictions of molecular length, and dielectric spectra (PDF)

AUTHOR INFORMATION

Corresponding Author

Jennifer L. Schaefer — Department of Chemical and Biomolecular Engineering, University of Notre Dame, Notre Dame, Indiana 46556, United States; orcid.org/0000-0003-4293-6328; Email: Jennifer.L.Schaefer.43@nd.edu

Autho

Jiacheng Liu — Department of Chemical and Biomolecular Engineering, University of Notre Dame, Notre Dame, Indiana 46556, United States; ⊚ orcid.org/0000-0001-9040-8656

Complete contact information is available at: https://pubs.acs.org/10.1021/acs.macromol.2c02516

Notes

The authors declare no competing financial interest.

ACKNOWLEDGMENTS

The authors gratefully acknowledge financial support from the National Science Foundation via award number DMR-1654162. The authors also acknowledge Dr. Phillip D. Pickett and the National Institute of Standards at Technology for sizeexclusion chromatography; Dr. Xiaobing Zuo at Advanced Photon Source beamline 12-ID-B at Argonne National Laboratory for assistance with X-ray scattering; Prof. Ruilan Guo from the Department of Chemical and Biomolecular Engineering at the University of Notre Dame for use of DSC instrumentation; the University of Notre Dame Center for Environmental Science and Technology (CEST) for ICP-OES instrumentation; and the University of Notre Dame Magnetic Resonance Research Center for NMR instrumentation. This research used resources of the Advanced Photon Source, a U.S. Department of Energy (DOE) Office of Science User Facility operated for the DOE Office of Science by Argonne National Laboratory under Contract No. DE-AC02-06CH11357.

REFERENCES

- (1) Kim, T.; Song, W.; Son, D. Y.; Ono, L. K.; Qi, Y. Lithium-Ion Batteries: Outlook on Present, Future, and Hybridized Technologies. *J. Mater. Chem. A* **2019**, *7*, 2942–2964.
- (2) Han, X.; Lu, L.; Zheng, Y.; Feng, X.; Li, Z.; Li, J.; Ouyang, M. A review on the key issues of the lithium ion battery degradation among the whole life cycle. *eTransportation* **2019**, *1*, No. 100005.
- (3) Zhao, Q.; Stalin, S.; Zhao, C. Z.; Archer, L. A. Designing Solid-State Electrolytes for Safe, Energy-Dense Batteries. *Nat. Rev. Mater.* **2020**, *5*, 229–252.
- (4) Angell, C. A. Superionic and Superacidic Glasses, Liquids and Plastic Crystals. ECS Meet. Abstr. 2010, MA2010-02, No. 2208.
- (5) Agrawal, R. C.; Gupta, R. K. Superionic solid: composite electrolyte phase an overview. *J. Mater. Sci.* **1999**, 34, 1131–1162.
- (6) Albertus, P.; Anandan, V.; Ban, C.; Balsara, N.; Belharouak, I.; Buettner-Garrett, J.; Chen, Z.; Daniel, C.; Doeff, M.; Dudney, N. J.; Dunn, B.; Harris, S. J.; Herle, S.; Herbert, E.; Kalnaus, S.; Libera, J. A.; Lu, D.; Martin, S.; McCloskey, B. D.; McDowell, M. T.; Meng, Y. S.; Nanda, J.; Sakamoto, J.; Self, E. C.; Tepavcevic, S.; Wachsman, E.; Wang, C.; Westover, A. S.; Xiao, J.; Yersak, T. Challenges for and Pathways toward Li-Metal-Based All-Solid-State Batteries. *ACS Energy Lett.* 2021, 6, 1399–1404.
- (7) Bocharova, V.; Sokolov, A. P. Perspectives for Polymer Electrolytes: A View from Fundamentals of Ionic Conductivity. *Macromolecules* **2020**, *53*, 4141–4157.
- (8) Gao, J.; Wang, C.; Han, D. W.; Shin, D. M. Single-Ion Conducting Polymer Electrolytes as a Key Jigsaw Piece for next-Generation Battery Applications. *Chem. Sci.* **2021**, *12*, 13248–13272.
- (9) Hall, L. M.; Stevens, M. J.; Frischknecht, A. L. Dynamics of Model Ionomer Melts of Various Architectures. *Macromolecules* **2012**, 45, 8097–8108.
- (10) Bolintineanu, D. S.; Stevens, M. J.; Frischknecht, A. L. Atomistic Simulations Predict a Surprising Variety of Morphologies in Precise Ionomers. *ACS Macro Lett.* **2013**, *2*, 206–210.
- (11) Bollinger, J. A.; Stevens, M. J.; Frischknecht, A. L. Quantifying Single-Ion Transport in Percolated Ionic Aggregates of Polymer Melts. ACS Macro Lett. **2020**, *9*, 583–587.
- (12) Frischknecht, A. L.; Paren, B. A.; Middleton, L. R.; Koski, J. P.; Tarver, J. D.; Tyagi, M.; Soles, C. L.; Winey, K. I. Chain and Ion Dynamics in Precise Polyethylene Ionomers. *Macromolecules* **2019**, 52, 7939–7950.
- (13) Hall, L. M.; Seitz, M. E.; Winey, K. I.; Opper, K. L.; Wagener, K. B.; Stevens, M. J.; Frischknecht, A. L. Ionic Aggregate Structure in Ionomer Melts: Effect of Molecular Architecture on Aggregates and the Ionomer Peak. J. Am. Chem. Soc. 2012, 134, 574–587.

- (14) Hall, L. M.; Stevens, M. J.; Frischknecht, A. L. Effect of Polymer Architecture and Ionic Aggregation on the Scattering Peak in Model Ionomers. *Phys. Rev. Lett.* **2011**, *106*, No. 127801.
- (15) Abbott, L. J.; Buss, H. G.; Thelen, J. L.; Mccloskey, B. D.; Lawson, J. W. Polyanion Electrolytes with Well-Ordered Ionic Layers in Simulations and Experiment. *Macromolecules* **2019**, *52*, 5518–5528.
- (16) Gainaru, C.; Stacy, E. W.; Bocharova, V.; Gobet, M.; Holt, A. P.; Saito, T.; Greenbaum, S.; Sokolov, A. P. Mechanism of Conductivity Relaxation in Liquid and Polymeric Electrolytes: Direct Link between Conductivity and Diffusivity. *J. Phys. Chem. B* **2016**, 120, 11074–11083.
- (17) Rank, C.; Yan, L.; Mecking, S.; Winey, K. I. Periodic Polyethylene Sulfonates from Polyesterification: Bulk and Nanoparticle Morphologies and Ionic Conductivities. *Macromolecules* **2019**, 52, 8466–8475.
- (18) Yan, L.; Hauler, M.; Bauer, J.; Mecking, S.; Winey, K. I. Monodisperse and Telechelic Polyethylenes Form Extended Chain Crystals with Ionic Layers. *Macromolecules* **2019**, *52*, 4949–4956.
- (19) Yan, L.; Hoang, L.; Winey, K. I. Ionomers from Step-Growth Polymerization: Highly Ordered Ionic Aggregates and Ion Conduction. *Macromolecules* **2020**, *53*, 1777–1784.
- (20) Park, J.; Staiger, A.; Mecking, S.; Winey, K. I. Sub-3-Nanometer Domain Spacings of Ultrahigh-χ Multiblock Copolymers with Pendant Ionic Groups. *ACS Nano* **2021**, *15*, 16738–16747.
- (21) Yan, L.; Rank, C.; Mecking, S.; Winey, K. I. Gyroid and Other Ordered Morphologies in Single-Ion Conducting Polymers and Their Impact on Ion Conductivity. *J. Am. Chem. Soc.* **2020**, *142*, 857–866.
- (22) Park, J.; Staiger, A.; Mecking, S.; Winey, K. I. Ordered Nanostructures in Thin Films of Precise Ion-Containing Multiblock Copolymers. *ACS Cent. Sci.* **2022**, *8*, 388–393.
- (23) Park, J.; Staiger, A.; Mecking, S.; Winey, K. I. Enhanced Li-Ion Transport through Selectively Solvated Ionic Layers of Single-Ion Conducting Multiblock Copolymers. *ACS Macro Lett.* **2022**, *11*, 1008–1013.
- (24) Liu, J.; Pickett, P. D.; Park, B.; Upadhyay, S. P.; Orski, S. V.; Schaefer, J. L. Non-Solvating, Side-Chain Polymer Electrolytes as Lithium Single-Ion Conductors: Synthesis and Ion Transport Characterization. *Polym. Chem.* **2020**, *11*, 461–471.
- (25) Liu, J.; Yang, L.; Pickett, P. D.; Park, B.; Schaefer, J. L. Li+Transport in Single-Ion Conducting Side-Chain Polymer Electrolytes with Nanoscale Self-Assembly of Ordered Ionic Domains. *Macromolecules* **2022**, *55*, 7752–7762.
- (26) Mark, J. E. Physical Properties of Polymers Handbook, 2nd ed.; Springer: New York, 2007.
- (27) Hiller, S.; Pascui, O.; Budde, H.; Kabisch, O.; Reichert, D.; Beiner, M. Nanophase Separation in Side Chain Polymers: New Evidence from Structure and Dynamics. *New J. Phys.* **2004**, *6*, No. 10. (28) Beiner, M.; Huth, H. Nanophase separation and hindered glass
- transition in side-chain polymers. *Nat. Mater.* **2003**, *2*, 595–599.
- (29) Agapov, A. L.; Wang, Y.; Kunal, K.; Robertson, C. G.; Sokolov, A. P. Effect of Polar Interactions on Polymer Dynamics. *Macromolecules* **2012**, *45*, 8430–8437.
- (30) Trigg, E. B.; Stevens, M. J.; Winey, K. I. Chain Folding Produces a Multilayered Morphology in a Precise Polymer: Simulations and Experiments. *J. Am. Chem. Soc.* **2017**, *139*, 3747–3755.
- (31) Holzwarth, U.; Gibson, N. The Scherrer Equation versus the "Debye-Scherrer Equation.". *Nat. Nanotechnol.* **2011**, *6*, No. 534.
- (32) Uchida, M.; McCoy, K.; Fukuto, M.; Yang, L.; Yoshimura, H.; Miettinen, H. M.; LaFrance, B.; Patterson, D. P.; Schwarz, B.; Karty, J. A.; Prevelige, P. E.; Lee, B.; Douglas, T. Modular Self-Assembly of Protein Cage Lattices for Multistep Catalysis. *ACS Nano* **2018**, *12*, 942–953.
- (33) Goossens, K.; Lava, K.; Bielawski, C. W.; Binnemans, K. Ionic Liquid Crystals: Versatile Materials. *Chem. Rev.* **2016**, *116*, 4643–4807
- (34) Wiesenauer, B. R.; Gin, D. L. Nanoporous Polymer Materials Based on Self-Organized, Bicontinuous Cubic Lyotropic Liquid

- Crystal Assemblies and Their Applications. *Polym. J.* **2012**, *44*, 461–468.
- (35) Park, J.; Staiger, A.; Mecking, S.; Winey, K. I. Structure-Property Relationships in Single-Ion Conducting Multiblock Copolymers: A Phase Diagram and Ionic Conductivities. *Macromolecules* **2021**, *54*, 4269–4279.
- (36) Arbe, A.; Genix, A.; Colmenero, J.; Richter, D.; Fouquet, P. Anomalous Relaxation of Self-Assembled Alkyl Nanodomains in High-Order Poly (n-Alkyl Methacrylates). *Soft Matter* **2008**, *4*, 1792–1795.
- (37) Jonscher, A. K. Dielectric Relaxation in Solids. J. Phys. D: Appl. Phys. 1999, 32, R57–R70.
- (38) Fan, F.; Wang, Y.; Sokolov, A. P. Ionic Transport, Microphase Separation, and Polymer Relaxation in Poly(Propylene Glycol) and Lithium Perchlorate Mixtures. *Macromolecules* **2013**, *46*, 9380–9389.
- (39) Mizuno, F.; Belieres, J. P.; Kuwata, N.; Pradel, A.; Ribes, M.; Angell, C. A. Highly Decoupled Ionic and Protonic Solid Electrolyte Systems, in Relation to Other Relaxing Systems and Their Energy Landscapes. *J. Non-Cryst. Solids* **2006**, *352*, 5147–5155.
- (40) Sangoro, J. R.; Iacob, C.; Serghei, A.; Friedrich, C.; Kremer, F. Universal Scaling of Charge Transport in Glass-Forming Ionic Liquids. *Phys. Chem. Chem. Phys.* **2009**, *11*, 913–916.
- (41) Wojnarowska, Z.; Feng, H.; Fu, Y.; Cheng, S.; Carroll, B.; Kumar, R.; Novikov, V. N.; Kisliuk, A. M.; Saito, T.; Kang, N. G.; Mays, J. W.; Sokolov, A. P.; Bocharova, V. Effect of Chain Rigidity on the Decoupling of Ion Motion from Segmental Relaxation in Polymerized Ionic Liquids: Ambient and Elevated Pressure Studies. *Macromolecules* **2017**, *50*, 6710–6721.
- (42) Angell, C. A. Fast Ion Motion in Glassy and Amorphous Materials. *Solid State Ionics* **1983**, *9*–10, 3–16.
- (43) Fan, F.; Wang, Y.; Hong, T.; Heres, M. F.; Saito, T.; Sokolov, A. P. Ion Conduction in Polymerized Ionic Liquids with Different Pendant Groups. *Macromolecules* **2015**, *48*, 4461–4470.
- (44) Angell, C. A. Dynamic Processes in Ionic Glasses. *Chem. Rev.* **1990**, *90*, 523–542.
- (45) Wang, Y.; Agapov, A. L.; Fan, F.; Hong, K.; Yu, X.; Mays, J.; Sokolov, A. P. Decoupling of Ionic Transport from Segmental Relaxation in Polymer Electrolytes. *Phys. Rev. Lett.* **2012**, *108*, No. 088303.
- (46) Do, C.; Lunkenheimer, P.; Diddens, D.; Götz, M.; Weiß, M.; Loidl, A.; Sun, X. G.; Allgaier, J.; Ohl, M. Li+ Transport in Poly(Ethylene Oxide) Based Electrolytes: Neutron Scattering, Dielectric Spectroscopy, and Molecular Dynamics Simulations. *Phys. Rev. Lett.* **2013**, *111*, No. 018301.
- (47) Choi, U. H.; Lee, M.; Wang, S.; Liu, W.; Winey, K. I.; Gibson, H. W.; Colby, R. H. Ionic Conduction and Dielectric Response of Poly(Imidazolium Acrylate) Ionomers. *Macromolecules* **2012**, *45*, 3974–3985.
- (48) Choi, U. H.; Mittal, A.; Price, T. L.; Gibson, H. W.; Runt, J.; Colby, R. H. Polymerized Ionic Liquids with Enhanced Static Dielectric Constants. *Macromolecules* **2013**, *46*, 1175–1186.
- (49) Stacy, E. W.; Gainaru, C. P.; Gobet, M.; Wojnarowska, Z.; Bocharova, V.; Greenbaum, S. G.; Sokolov, A. P. Fundamental Limitations of Ionic Conductivity in Polymerized Ionic Liquids. *Macromolecules* **2018**, *51*, 8637–8645.
- (50) Bartels, J.; Hess, A.; Shiau, H. S.; Allcock, H. R.; Colby, R. H.; Runt, J. Synthesis, Morphology, and Ion Conduction of Polyphosphazene Ammonium Iodide Ionomers. *Macromolecules* **2015**, *48*, 111–118.
- (51) Paren, B. A.; Nguyen, N.; Ballance, V.; Hallinan, D. T.; Kennemur, J. G.; Winey, K. I. Superionic Li-Ion Transport in a Single-Ion Conducting Polymer Blend Electrolyte. *Macromolecules* **2022**, *55*, 4692–4702.
- (52) Wang, W.; Tudryn, G. J.; Colby, R. H.; Winey, K. I. Thermally Driven Ionic Aggregation in Poly(Ethylene Oxide)-Based Sulfonate Ionomers. *J. Am. Chem. Soc.* **2011**, *133*, 10826–10831.
- (53) Wheatle, B. K.; Lynd, N. A.; Ganesan, V. Effect of Polymer Polarity on Ion Transport: A Competition between Ion Aggregation

- and Polymer Segmental Dynamics. ACS Macro Lett. 2018, 7, 1149–1154.
- (54) Namikawa, H. Multichannel Conduction in Alkali Silicate Glasses. *J. Non-Cryst. Solids* **1974**, *14*, 88–100.
- (55) Namikawa, H. Characterization of the Diffusion Process in Oxide Glasses Based on the Correlation between Electric Conduction and Dielectric Relaxation. *J. Non-Cryst. Solids* **1975**, *18*, 173–195.
- (56) Macdonald, J. R. Addendum to "Fundamental Questions Relating to Ion Conduction in Disordered Solids.". *J. Appl. Phys.* **2010**, *107*, No. 101101.

□ Recommended by ACS

Impact of Ionic Correlations on Selective Salt Transport in Ligand-Functionalized Polymer Membranes

Harnoor Singh Sachar, Venkat Ganesan, et al.

MARCH 01, 2023 MACROMOLECULES

READ 🗹

ToF-SIMS Depth Profiling to Measure Nanoparticle and Polymer Diffusion in Polymer Melts

Kaitlin Wang, Karen I. Winey, et al.

MARCH 16, 2023

MACROMOLECULES

READ 🗹

Boronic Ester Transesterification Accelerates Ion Conduction for Comb-like Solid Polymer Electrolytes

Hongli Wang, Zhigang Xue, et al.

MARCH 06, 2023

MACROMOLECULES

READ 🗹

Bisphenol-Derived Single-Ion Conducting Multiblock Copolymers as Lithium Battery Electrolytes: Impact of the Bisphenol Building Block

Alexander Mayer, Dominic Bresser, et al.

MARCH 17, 2023

MACROMOLECULES

READ 🗹

Get More Suggestions >